




















RESEARCH ARTICLE | AUGUST 02 2021

Demonstration of an x-ray Raman spectroscopy setup to study warm dense carbon at the high energy density instrument of European XFEL

K. Voigt ; M. Zhang; K. Ramakrishna ; A. Amouretti; K. Appel ; E. Brambrink; V. Cerantola ; D. Chekrygina ; T. Döppner ; R. W. Falcone; K. Falk ; L. B. Fletcher; D. O. Gericke ; S. Göde; M. Harmand ; N. J. Hartley ; S. P. Hau-Riege; L. G. Huang; O. S. Humphries ; M. Lokamani ; M. Makita; A. Pelka; C. Prescher; A. K. Schuster ; M. Šmíd ; T. Toncian ; J. Vorberger ; U. Zastra ; T. R. Preston; D. Kraus 




Phys. Plasmas 28, 082701 (2021)
<https://doi.org/10.1063/5.0048150>



APL Machine Learning

2023 Papers with Best Practices in Data Sharing and Comprehensive Background

[Read Now](#)



Demonstration of an x-ray Raman spectroscopy setup to study warm dense carbon at the high energy density instrument of European XFEL

Cite as: Phys. Plasmas **28**, 082701 (2021); doi: 10.1063/5.0048150

Submitted: 22 February 2021 · Accepted: 20 June 2021 ·

Published Online: 2 August 2021



View Online



Export Citation



CrossMark

K. Voigt,^{1,2,a)}  M. Zhang,^{1,3}  K. Ramakrishna,^{1,2,4}  A. Amouretti,⁵  K. Appel,⁶  E. Brambrink,⁶  V. Cerantola,⁶  D. Chekrygina,⁷  T. Döppner,⁸  R. W. Falcone,⁹  K. Falk,^{1,2,10}  L. B. Fletcher,¹¹  D. O. Gericke,¹²  S. Göde,⁶  M. Harmand,⁵  N. J. Hartley,^{1,11}  S. P. Hau-Riege,⁸  L. G. Huang,¹  O. S. Humphries,¹  M. Lokamani,¹  M. Makita,⁶  A. Pelka,¹  C. Prescher,¹³  A. K. Schuster,^{1,2}  M. Šmíd,¹  T. Toncian,¹  J. Vorberger,¹  U. Zastrau,⁶  T. R. Preston,⁶ and D. Kraus^{1,14,b)} 

AFFILIATIONS

¹Helmholtz-Zentrum Dresden-Rossendorf, Bautzner Landstraße 400, 01328 Dresden, Germany

²Technische Universität Dresden, 01069 Dresden, Germany

³Institute of Physical Science and Information Technology, Anhui University, Hefei 230601, China

⁴Center for Advanced Systems Understanding (CASUS), 02826 Görlitz, Germany

⁵Institut de Minéralogie, de Physique des Matériaux et de Cosmochimie, Sorbonne Université, 75005 Paris, France

⁶European XFEL, Holzkoppel 4, 22869 Schenefeld, Germany

⁷Scientific Computing Department, Rutherford Appleton Laboratory, Science and Technology Facilities Council, Harwell Campus, Oxfordshire OX11 0QX, United Kingdom

⁸Lawrence Livermore National Laboratory, Livermore, California 94550, USA

⁹Department of Physics, University of California, Berkeley, California 94720, USA

¹⁰Institute of Physics of the ASCR, 182 21 Prague, Czech Republic

¹¹SLAC National Accelerator Laboratory, Menlo Park, California 94025, USA

¹²Centre for Fusion, Space and Astrophysics, Department of Physics, University of Warwick, Coventry CV4 7AL, United Kingdom

¹³Deutsches Elektronen-Synchrotron DESY, Notkestraße 85, 22607 Hamburg, Germany

¹⁴Institut für Physik, Universität Rostock, Albert-Einstein-Str. 23, 18059 Rostock, Germany

^{a)}Author to whom correspondence should be addressed: k.voigt@hzdr.de

^{b)}Electronic mail: dominik.kraus@uni-rostock.de

ABSTRACT

We present a proof-of-principle study demonstrating x-ray Raman Spectroscopy (XRS) from carbon samples at ambient conditions in conjunction with other common diagnostics to study warm dense matter, performed at the high energy density scientific instrument of the European x-ray Free Electron Laser (European XFEL). We obtain sufficient spectral resolution to identify the local structure and chemical bonding of diamond and graphite samples, using highly annealed pyrolytic graphite spectrometers. Due to the high crystal reflectivity and XFEL brightness, we obtain signal strengths that will enable accurate XRS measurements in upcoming pump-probe experiments with a high repetition-rate, where the samples will be pumped with high-power lasers. Molecular dynamics simulations based on density functional theory together with XRS simulations demonstrate the potential of this technique and show predictions for high-energy-density conditions. Our setup allows simultaneous implementation of several different diagnostic methods to reduce ambiguities in the analysis of the experimental results, which, for warm dense matter, often relies on simplifying model assumptions. The promising capabilities demonstrated here provide unprecedented insights into chemical and structural dynamics in warm dense matter states of light elements, including conditions similar to the interiors of planets, low-mass stars, and other celestial bodies.

© 2021 Author(s). All article content, except where otherwise noted, is licensed under a Creative Commons Attribution (CC BY) license (<http://creativecommons.org/licenses/by/4.0/>). <https://doi.org/10.1063/5.0048150>

I. MOTIVATION

Warm dense matter (WDM), an extreme material state with temperatures on the order of several thousand to several million kelvin and solid densities, poses severe challenges for its characterization.¹ Reliable experiments in the laboratory are technologically demanding, since WDM can only be investigated as a highly transient and optically opaque state in a small sample volume.² Providing a precise theoretical description of WDM is extremely challenging due to the complex interplay of many effects, which act on similar energy scale, including partial ionization, strong ion-ion coupling, and electron degeneracy.³ The development of new models is required, as it is not feasible to apply well-established concepts from condensed matter or plasma physics theory. The investigation of light elements like carbon and carbon-containing materials in their WDM conditions is, among others, highly relevant to planetary and stellar physics.^{4–6} Warm dense carbon is expected to play a prominent role inside icy giant planets contributing to the planets' energy balance via diamond precipitation and to their peculiar magnetic field structure via liquid metallic carbon.⁷ Aside from that, carbon is a very practical material for WDM research, as a low-Z material having a computationally tractable electron number. It is also convenient to handle in the laboratory, as a non-hazardous solid sample material, that is available in various structures and densities.

Experimentally, one method to generate WDM employs laser-driven shock compression, where a high-energy high-intensity laser with nanosecond pulse duration is focused onto a bulk sample to drive a shock wave which compresses the material. For a few nanoseconds, high-pressure states up to the order of 100 GPa with temperatures on the order of 1 eV can be generated with this technique.^{8–12} WDM states have also been accessed with isochoric heating schemes using high-intensity fs-lasers, FEL pulses, and highly energetic particle beams.^{13–19} Probing these dense and transient states requires a volume-penetrating and ultra-short pulsed backlighter with high brilliance and pulse lengths shorter than a nanosecond. For that reason, modern x-ray sources like synchrotrons and x-ray free electron lasers (XFELs) in combination with high-energy and high-intensity lasers have become important facilities for conducting WDM experiments. Furthermore, various x-ray diagnostics have been developed as powerful tools for the characterization of WDM states in the laboratory. Experimental techniques including x-ray diffraction (XRD),^{5,20} x-ray absorption spectroscopy (XAS),^{8–10,15} small angle x-ray scattering (SAXS),^{14,21} and spectrally resolved collective (forward) and non-collective (backward) x-ray Thomson scattering (XRTS)^{18,22–27} have been applied to gain insight into plasma conditions and dynamics. While diffraction methods are able to give insight into the global ionic structure, information about the local structure, electronic structure, and chemical bonding can be obtained with x-ray absorption near-edge structure (XANES) and extended x-ray absorption fine structure (EXAFS) spectroscopy. Spectrally resolved XRTS techniques can probe important properties like the electron temperature and density and the ionization state as well as plasmon features. SAXS provides the opportunity to observe plasma dynamics at nm length scales. The data analysis of all the aforementioned diagnostics requires theoretical input. Therefore, a combination of multiple complementary diagnostics is desirable to reduce the uncertainties introduced by the approximate theoretical models and experimental errors.^{21,28,29}

Due to its importance and practicality, carbon and carbon containing samples are popular materials to study in WDM experiments.^{5,28,30,31} While the combination of XRTS, SAXS, and XRD measurements in shock compression experiments has resulted in outstanding findings in recent years,^{21,27} it is challenging to adapt experimental setups to include XAS for low-Z materials, which have K-edge energies in the soft x-ray regime.³² X-rays with energies below 1 keV typically penetrate only surface layers or very thin samples with sub-micrometer thicknesses. In experiments using dynamic shock compression techniques with a high-energy laser and nanosecond pulse length, thicker bulk samples (10–100 μm) are required to reach the relevant pressure conditions as well as to match the shock transition times inside the sample with the pulse length of the laser. A promising alternative, which overcomes the difficulties in XAS transmission measurements on low-Z materials, is x-ray Raman scattering, which can provide similar information.

X-ray Raman spectroscopy (XRS) studies the non-resonant inelastic x-ray scattering from the core electrons while transferring parts of the incident x-ray energy and exciting the electrons to higher level unoccupied states.^{33,34} The cross section for scattering from the ground state $|i\rangle$ with the energy E_i to the final state $|f\rangle$ with the energy E_f is proportional to the dynamic structure factor given by

$$S(q, \omega) = \sum_f |\langle i | e^{-iq \cdot r} | f \rangle|^2 \delta(\hbar\omega + E_i - E_f),$$

with q being the momentum transfer, $\hbar\omega$ the transferred energy, and r the radius of the core orbital.³⁵ Investigating the spectrum of the energy loss of the x-ray photons and not the absorption of the incident x-ray energy allows the use of hard x-rays, which can penetrate and probe the bulk of the sample material. XRS measurements have been performed for decades at various beamlines of several synchrotron sources on samples at ambient conditions but also with compressed material in diamond anvil cell experiments.^{33,34,36–41} However, a typical synchrotron setup, e.g., using high-resolution diced analyzer crystals and scanning the photon energy, is not practical for most WDM experiments where additional diagnostics usually require the photon energy to remain constant.

In this work, we show that comparable measurements can be obtained at x-ray free electron laser sources in experimental setups including additional drive options to study WDM under high-temperature high-pressure environments. The combination of XRS with other already existing spectrally resolved x-ray scattering techniques is relatively straightforward. Since the non-collective x-ray scattering spectrum shows the superposition of the different contribution from elastic and inelastic scattering at the free, valence, and core electrons, it is possible to extract spectra for studying the bound-free transitions from core electrons with a few adjustments to the usual experimental procedure.¹⁸ The main challenges are the extremely low cross section of the hard x-ray scattering from core electrons and the energy resolution required to resolve structures in the XRS spectrum.^{33,34} This can be overcome by data accumulation of multiple shots in high-repetition rate experiments at XFELs using bright, low bandwidth x-ray pulses together with high-resolution and highly reflective spectrometers in carefully designed experimental setups. To keep the background from the scattering from valence electrons as low as possible, the position of the maximum of the Compton peak can be varied by the choice of the investigated momentum transfer by

adjusting either the incident x-ray energy or the scattering angle.^{33,34} At low q , when $q \cdot r \ll 1$, mainly dipole transitions are investigated; here, the dynamical structure factor can be expressed as

$$S(q, \omega)_{dipole} = \sum_f q^2 |\langle i|r|f \rangle|^2 \delta(\hbar\omega + E_i - E_f),$$

and the XRS spectrum becomes equivalent to the x-ray absorption spectrum.^{35,36} At higher momentum transfer, also non-dipole transitions can be probed.^{34,42,43} In addition, the XRS intensity can also be optimized to a certain extent by the choice of q , due to its quadratic dependence on the momentum transfer.⁴² A first attempt of studying the carbon K-edge in non-collective scattering spectra of isochorically heated carbon (pyrolytic graphite) was performed in 2014 at the Linac Coherent Light Source (LCLS).¹⁸ While edge-shifts due to ionization potential depression in dense matter could be observed in this experiment, the energy resolution of 20 eV, resulting from the spectrometer resolution and the XFEL bandwidth, did not allow the investigation of the substructures in the XRS signal. Here, we present a proof-of-principle experiment, where carbon samples were probed at ambient conditions, achieving energy resolutions of ~ 1 eV while taking advantage of the high brightness of the European XFEL. Additionally, we show theoretical predictions using density functional theory molecular dynamics (DFT-MD) and XRS simulations demonstrating the potential for experiments using rep-rated drive systems.

II. EXPERIMENT

The experiment was performed at the High-Energy-Density (HED) scientific instrument of the European x-ray free electron laser.⁴⁴ An x-ray only setup was used to demonstrate the capability for XRS measurements at HED, to be extended in conjunction with planned future laser drivers once they come online.⁴⁵ The experimental setup is presented in Fig. 1.

We investigated polycrystalline carbon foils in the form of diamond and graphite (flexible, rigid, and pyrolytic) with thicknesses ranging from 10 to 125 μm and densities ranging from 0.9 to 3.51 g cm^{-3} . X-ray pulses with a photon energy of 6 keV were focused by compound refractive Be lenses to spot sizes $< 20 \mu\text{m}$ onto the

carbon samples. The energy bandwidth of the x-ray beam was reduced from the full self-amplified spontaneous emission (SASE) spectrum to < 1 eV using a four-bounce Si-111 monochromator⁴⁶ to ensure the required high spectral resolution of the measurements. The transmission of the monochromator was $\sim 1\%$ in this experiment, resulting in x-ray pulse energies of $\sim 20 \mu\text{J}$. The “1/e” absorption depth in carbon at 6 keV is $\sim 420 \mu\text{m}$, and therefore, most of the pulse energy is transmitted through the sample up to a maximum absorption of $\sim 20\%$ for 125 μm thick graphite. The average absorbed energy per electron was calculated to be on the order of 1 meV for all sample types, which indicates that heating effects by the x-rays are negligible for the resulting XRS spectrum.

The x-ray matter interaction is dominated by photoionization for the conditions present in this experiment, while the relative cross section for x-ray scattering is on the order of 1%. An angular dependent measurement further reduces the detected signal, but a careful choice of the detection angle also lowers the influence of the elastic scattering to the spectrum by avoiding Bragg reflections. The inelastic scattering spectrum is dominated by Compton scattered photons on the valence electrons in the L-shell of the carbon atoms, and only a few photons per pulse contribute to the x-ray Raman signal. Data were collected using a highly annealed pyrolytic graphite (HAPG) crystal spectrometer⁴⁷ in a von Hámos geometry coupled to a JUNGFRAU 2D pixel detector⁴⁸ to collect x-ray scattering spectra in backward direction at 155° . The cylindrically curved mosaic crystal (40 μm thickness, 80 mm radius of curvature) results in an efficient photon detection from divergent sources, enabling single photon detection at a spectral resolution of 2.7 eV at 6 keV. The scattering angle of 155° , corresponding to a momentum transfer of 5.94 \AA^{-1} , has been carefully chosen to avoid overlapping of the Compton peak maximum with the region of the binding energy of the core electrons, while ensuring a good signal-to-noise ratio for the XRS signal.^{33,34} Taking advantage of the exceptional high brightness of the XFEL beam and averaging over thousands of shots while using a repetition rate of the XFEL of 10 Hz, it was possible to record x-ray Raman spectra of different carbon samples, despite the extremely small cross section of the inelastic x-ray Raman scattering process.

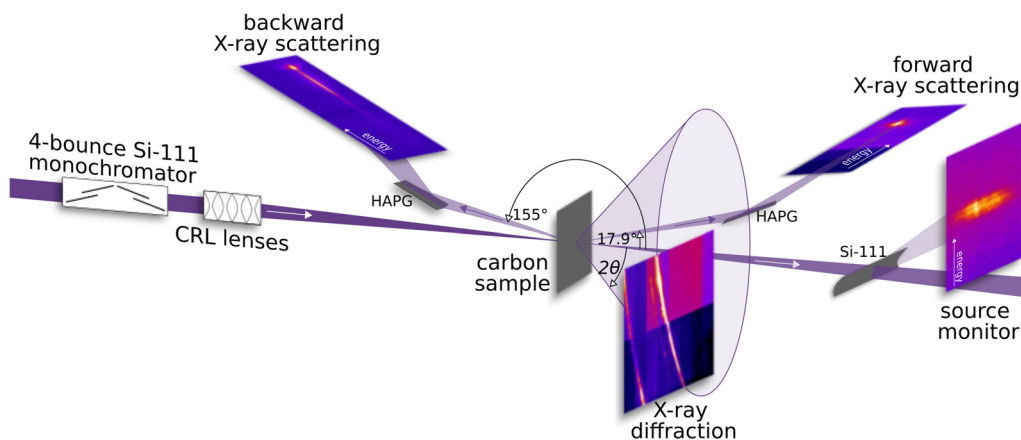


FIG. 1. Schematic illustration of the experimental setup: carbon containing samples are irradiated by monochromatic x-rays of 6 keV, a curved mosaic HAPG spectrometer in von-Hamos geometry is set up in backward direction at 155° as the main diagnostic presented in this article. Additional diagnostics are setup in the downstream direction together with the source monitor measuring the spectrum of the transmitted x-rays.

A similar setup like for the backward scattering measurements has been installed in the forward direction at an angle of 18° . A thicker HAPG crystal ($100\ \mu\text{m}$) provides higher signal but lower energy resolution collected on an ePix100 detector.⁴⁹ The transmitted x-rays were investigated using a bent Si-111 crystal spectrometer and an Andor Zyla 5.5 sCMOS detector⁵⁰ downstream of the interaction to measure the source spectrum. An *in situ* angular resolving XRD measurement was collected on an ePix100 detector⁴⁹ to obtain structural information from the sample.

All diagnostics with the exception of the downstream source monitor were contained within the vacuum chamber. Example detector images are shown in Fig. 1. All diagnostics were capable of running simultaneously, providing extensive on-shot characterization of the samples. The primary focus of this work is the analysis of the backward scattering spectrometer and discussion of the future possibilities to utilize XRS for WDM research.

III. RESULTS

Figure 2 shows a backward x-ray scattering spectrum recorded from a diamond sample ($10\ \mu\text{m}$ thickness) at ambient conditions with and without using an inserted four-bounce Si-111 monochromator in the x-ray beamline. The energy calibration was carried out using the $K\alpha$ and $K\beta$ x-ray emission lines from chromium samples. The presented spectra are normalized to the Compton peak maximum to account for shot-to-shot variations in x-ray flux, sample thicknesses, and materials. To reduce the detector noise, all pixels whose values were below a threshold corresponding to the single-photon event were discarded, before averaging over the whole data set. Due to the low transmission of the monochromator and therefore the low x-ray flux, $\sim 18\,000$ shots were accumulated for the scattering spectrum, compared to the average of ~ 90 shots for obtaining a representative spectrum without monochromating the x-rays. In both cases, the carbon K-edge resulting from scattering from core electrons is clearly visible as a peak in the spectrum at $\sim 5715\ \text{eV}$. The downshift of $\sim 285\ \text{eV}$ from the elastic peak (corresponding to the $1\ \text{s}$ binding energy) places the carbon K-edge at the low energy tail of the inelastic Compton scattering feature. Reducing the x-ray energy bandwidth further improves

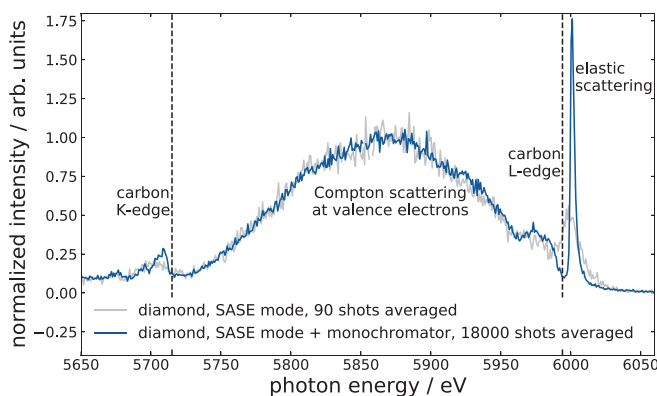


FIG. 2. Backward x-ray scattering spectrum from diamond normalized to the inelastic signal maximum. Gray: SASE mode (average x-ray pulse energy of $1650\ \mu\text{J}$). Blue: monochromatic x-rays (average x-ray pulse energy of $17\ \mu\text{J}$). Dashed lines indicate the carbon K-edge at $\sim 285\ \text{eV}$ and L-edge energies at $\sim 6\ \text{eV}$ below the elastic scattering peak.

the data quality, enhancing the visibility of the L-edge features at $\sim 6\ \text{eV}$ below the elastic peak and substructures at the K-edge, which can be used for an x-ray Raman spectroscopy investigation.

We measured the total energy resolution by elastic scattering from a metallic glass sample (mixture of Co/Si/B/Fe/Ni, $18\ \mu\text{m}$ thick foil). The higher atomic number results in an enhanced intensity of elastic scattering, which allows for a decoupled analysis of the elastic scattering signal and neglecting the inelastic spectral features. The elastic scattering of hard x-rays can be estimated with a delta function in this work, since x-ray scattering from phonons is on the order of $100\ \text{meV}$.⁵¹ Therefore, the peak shape at $6\ \text{keV}$ of the elastic scattering signal, presented in Fig. 3 (left), can serve as a good approximation of the instrument function, which describes the broadening of the signal due to beamline and spectrometer contributions. The broadening due to beamline components is dominated by the x-ray bandwidth and can be estimated by measuring the source spectrum from transmitted photons (shown in Fig. 3, middle). A deconvolution of the source spectrum from the elastic scattering signal of the metallic glass allows determination of the transfer function between the two spectrometers (presented in Fig. 3, right), which represents—to a good approximation—the broadening of the elastic scattering due to spectrometer characteristics. The resolution of a HAPG crystal spectrometer is affected by the penetration of the x-rays into the depth of the crystal. This effect, so-called depth broadening, is energy dependent and causes the asymmetric peak shape.⁵² The transfer function is therefore modeled by a Gaussian function convolved with an exponential decay to obtain an estimate of the energy resolution of the HAPG spectrometer of $2.7\ \text{eV}$. This is in agreement with the recently published characterization of the HAPG von Hámos spectrometer at the HED instrument of the European XFEL.⁴⁷ Overall, the total energy resolution of the experiment is $3.3\ \text{eV}$ accounting for both broadening due to the spectrometer and the bandwidth of the monochromated XFEL (compared with $20.5\ \text{eV}$ in the SASE configuration).

With a precise determination of the transfer function, it is possible to extract the instrument function for all investigated samples in SASE mode and monochromated SASE mode by a convolution of the transfer function with the simultaneously measured source spectra. This allows for the deconvolution of the instrument function from the experimental scattering spectra to obtain the inelastic signal without instrumental broadening effects. However, a careful interpretation of the obtained results is necessary due to high frequency noise that is introduced by the deconvolution process.

Figure 4 shows the obtained x-ray Raman scattering spectrum as a function of the photon energy loss for a diamond sample after the deconvolution of the instrument function from the scattering spectrum. A linear function which represents the Compton background is subtracted in the region around the carbon K-edge. The obtained spectrum shows a good agreement with theoretical predictions calculated for ambient diamond using the FDMNES code^{53,54} (described in detail below in Sec. IV). Both experimental and calculated spectra reflect the main features arising from the electronic band structure: a lower set of conduction bands and a set of higher energy excited states separated by a dip around an energy transfer of $300\ \text{eV}$, which is associated with the second bandgap of diamond.^{42,55}

The achieved energy resolution allows the investigation of substructures in the x-ray Raman spectra, and in turn access to information about the chemical bonding of the investigated material. The

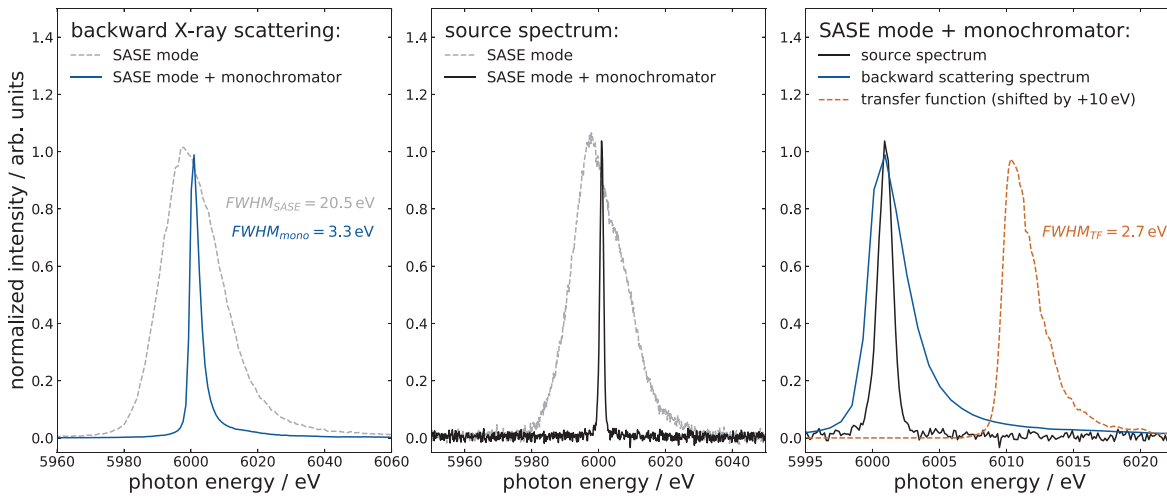


FIG. 3. Determination of the transfer function between the backward spectrometer and the source monitor by deconvolution of the source spectrum from the elastic scattering signal from a metallic glass sample. Left: elastic scattering signal in SASE mode (dashed gray) and with monochromatic x-rays (blue). Middle: source spectra in SASE mode (dashed gray) and with monochromatic x-rays (black). Right: transfer function (dashed orange, shifted by +10 eV relative to the elastic scattering peak) obtained by deconvolving the source spectrum (black) from the backward scattering spectrum (blue) both in the SASE mode with the monochromator.

carbon atoms in a diamond crystal form four equal σ -bonds due to sp^3 -hybridization, which results in the tetrahedral structure of the crystal. In graphite, the sp^2 -hybridization creates two-dimensional layers of σ -bonded hexagonal arranged carbon atoms, while the remaining electrons form weaker π -bonds connecting the planes. This difference in the chemical bond structure can be observed in the experimental x-ray Raman scattering spectra for different graphite samples and diamond presented in Fig. 5. Transitions of core electrons into the related unoccupied antibonding σ^* - and π^* -bands can be observed at energy transfers of 292 and 285 eV, respectively. While the spectrum of the diamond sample only shows σ -bonding, in all of the graphite spectra a clear peak associated with the π^* -band appears. Varying intensities of that peak can arise from different orientations of the graphite layers with respect to the polarization of the incoming x-ray beam.^{36,56} Due to a smaller accumulation of data shots in these

measurements, a Gaussian filter with $\sigma = 1.5$ was applied, which revealed the characteristic features of the XRS spectra. However, the data quality can be easily improved by collecting a larger number of data shots, as demonstrated with the spectrum from diamond samples. Nevertheless, the present state already allows the investigation of phase transitions and changes in the bond structure in carbon containing samples. Samples heated or compressed to WDM conditions will be possible in future experiments.

IV. SIMULATIONS

The XRS simulations for ambient conditions, that are presented in Fig. 4 for $q = 5.94 \text{ \AA}^{-1}$, have been performed using the Finite Difference Method Near Edge Structure (FDMNES) code^{53,54} for an ideal diamond lattice in a unit cell consisting of eight carbon atoms. The Schrödinger equation is solved self-consistently using a finite difference method for the electronic structure, evaluating the dipole matrix for a momentum transfer of $|\vec{q}| = 5.94 \text{ \AA}^{-1}$ up to the quantum number $l = 2$. Calculated XRS spectra for lower momentum transfers in a range of $1.0\text{--}4.0 \text{ \AA}^{-1}$ show a nearly identical shape compared to the spectrum of $q = 5.94 \text{ \AA}^{-1}$. This indicates that also at a moderate q of 5.94 \AA^{-1} dipole allowed transitions are dominating the spectrum, and it demonstrates the feasibility of XRS as an alternative to soft XAS measurements in the chosen q regime.

Density functional molecular dynamics (DFT-MD) simulations were carried out in combination with XRS simulations to provide a reference for the expected changes in the XRS signal of heated and compressed samples. To perform DFT-MD simulations, we used the Vienna *ab initio* simulation package (VASP)^{57–60} together with a Nosé–Hoover thermostat^{61,62} and a Perdew–Burke–Ernzerhof (PBE) functional⁶³ to calculate equilibrated ionic configurations. The simulations were run with a 0.2 fs time step up to a total time of at least 2 ps until thermal equilibration is achieved. The system consists of eight atoms sampled using a $2 \times 2 \times 2$ Monkhorst-Pack mesh⁶⁴ with a hard carbon projector augmented wave (PAW) pseudopotential. The

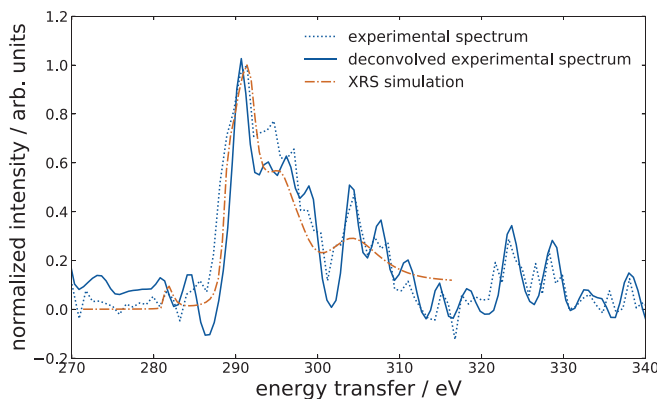


FIG. 4. Measured x-ray Raman spectrum pre- (dotted blue) and post- (continuous blue) deconvolution procedure compared with the calculated x-ray Raman spectrum (dashed orange) of a diamond sample.

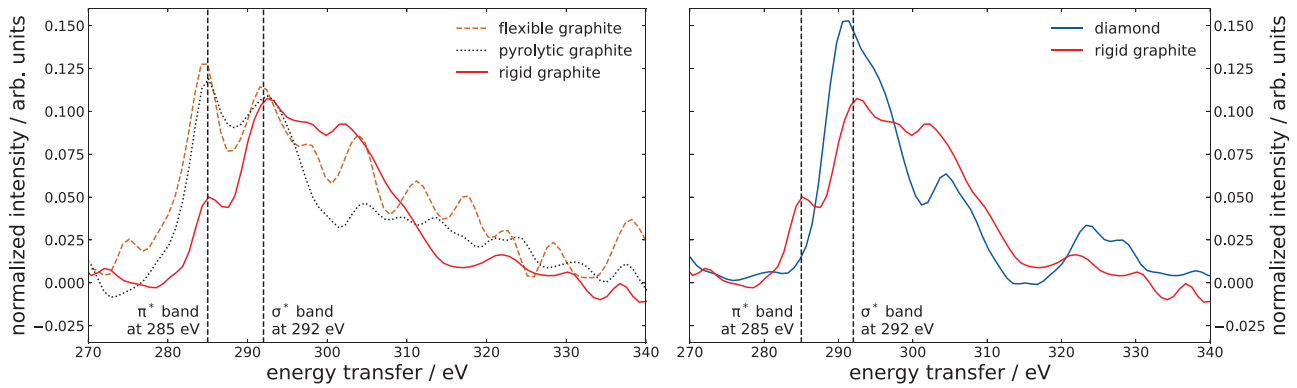


FIG. 5. Measured x-ray Raman spectra for different sample materials (smoothed data). The black dashed lines indicate the antibonding σ^* - and π^* -bands. Left: comparison of different graphite samples. Right: comparison between diamond and (rigid) graphite.

energy cutoff was set to 900 eV. We consistently increased the number of bands at higher temperatures to achieve convergence. The equilibrated snapshots obtained by DFT-MD simulations are used to perform the XRS calculations via FDMNES. Eight random ionic configurations are chosen, with which the XRS spectra for high temperatures were subsequently computed. The simulations for compressed conditions are performed based on the lattice parameters obtained using the Vinet equation of state for diamond at ambient temperature.^{65,66}

Figure 6 shows the obtained theoretical predictions for isochorically heated diamond samples for a range of temperatures from 0.5 to 7.5 eV as well as calculations for different pressure conditions from 150 to 437 GPa corresponding to densities of 4.4 to 5.5 g cm⁻³. The pressure increase results in a reduction of the peak intensities and shifts the spectral features toward higher energies. This is expected due to the increase in the direct and indirect bandgap of diamond with pressure.^{67,68} On the other hand, isochoric heating of diamond causes a gradual closure of the bandgap and the smoothing of the spectral features, due to an increasing disorder of the crystal's structure. Temperatures above ~0.5 eV result in the transition to the liquid state,⁶⁹ while the presented curves at a temperature of 0.5 eV represent the onset of the WDM regime. The combined simulation result, at 0.5 eV and 150 GPa, shows the competing effects of the bandgap opening at high pressures and their closure at high temperatures. This is clearly observable in comparison with the curve for the same temperature at ambient pressure.

The possibility of investigating phase transitions, as well as pressure and temperature effects on the electronic bonding structure, is corroborated by the theoretical predictions that clearly show the great potential of observing and analyzing XRS spectra of isochorically heated or compressed diamond samples in the WDM regime. In typical experimental setups at XFEL facilities, as presented here, we can now achieve sufficient energy resolution and data quality to be able to distinguish individual theoretical models by comparison with the experimental data. In particular, the simultaneous operation of additional methods like XRTS, XRD, and SAXS is promising.

V. SUMMARY

We have presented x-ray Raman scattering spectra of ambient diamond and graphite recorded at the HED instrument of the

European XFEL in an experimental setup well suited for future WDM experiments. The setup allows for a straightforward combination with multiple additional diagnostics, such as XRD, XRTS, and SAXS, that have been routinely fielded for WDM experiments, and can be adapted to perform experiments with different low-Z material samples besides carbon. The exceptionally high brightness of the

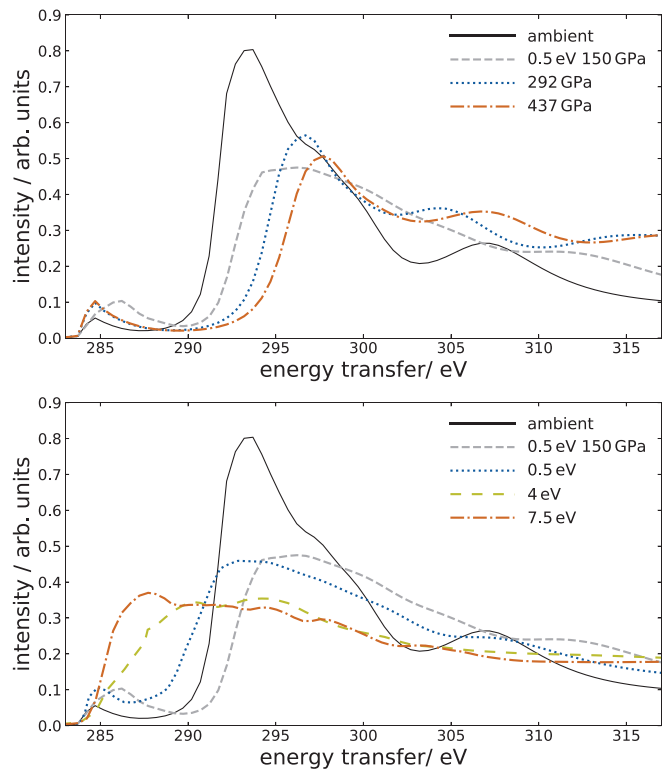


FIG. 6. Calculated XRS spectra for compressed and heated diamond for a momentum transfer of $q = 5.94 \text{ \AA}^{-1}$. For comparison, the spectrum for ambient conditions is shown in black. Top: different pressure conditions ranging from 150 to 437 GPa corresponding to densities of 4.4 to 5.5 g cm⁻³. Bottom: various temperature conditions ranging from 0.5 to 7.5 eV.

25 March 2024 09:14:55

European XFEL together with the high-resolution HAPG spectrometer made it possible to record full-range spectra within one x-ray pulse that is essential when investigating transient warm dense material states. However, an accumulation of multiple spectra is necessary to study substructures in the XRS signal due to the exceedingly small cross section of the x-ray Raman scattering process. We have presented, additionally, DFT-MD calculations in combination with XRS simulations that corroborate the great potential of the demonstrated setup observing samples at pressure and temperature conditions in the WDM regime.

Samples, that are pumped to WDM conditions, will be irreversibly damaged in each shot. Thus, very often single-shot measurements are required, which can be provided at HED in the shot-on-demand mode using a pulse picker. Alternatively, depending on the degree of damage, rapid raster scans are a great option to accumulate a large number of data shots, e.g., at x-ray heating experiments.⁷⁰ Moreover, high-repetition rate sample designs⁷¹ will be beneficial to manage the preparation of the required high amount of samples.

The accumulation of $\sim 10\,000$ shots per XRS spectrum in the experiment presented here was required due to the limited x-ray flux after insertion of the monochromator and is not foreseen to be a barrier to future experiments with a drive laser. An extensive alignment procedure of the monochromator could improve the flux by a factor of 2.5. However, being able to use the seeded x-ray beam^{72,73} in upcoming experiments will reduce the necessity to monochromate the x-ray beam, since the self-seeding process will itself reduce the bandwidth of the x-ray pulses without significantly decreasing the fluence. This will give approximately 50 times more x-ray photons hitting the sample, assuming pulse energies of ~ 1 mJ for the seeded x-ray pulse. This assumption is based on the best performance, at present, of the two-chicane seeding design of the European XFEL at a repetition rate of 10 Hz at 7.5 keV. In this configuration, a FWHM of 1.2(3) eV and pulse energies between 0.5 and 1.5 mJ, while obtaining a SASE background of ~ 140 μ J, have been achieved.⁷⁴ The scattering intensity can be further enhanced by increasing the thickness of the investigated samples. This will be naturally the case for samples used in a laser shock compression experiment, where sample thicknesses on the order of 100 μ m are often necessary. In total, this results in a reduction of the minimum number of accumulated shots per spectrum by an estimated factor of 500, so that averaging over tens of shots will be sufficient to reach similar data quality as in the spectra presented here. In a WDM experiment, a series of 10 to 20 spectra are usually recorded to cover various high-pressure and high-temperature conditions of the investigated sample material or to image the dynamics during the WDM creation process. Thus, a complete measurement will require on the order of a few thousand shots in total, which would be well within reach by using the high repetition rates of the European XFEL and the planned high-energy optical drive laser currently under construction at HED (DiPOLE-100X laser system⁷⁵).

ACKNOWLEDGMENTS

We acknowledge the European XFEL in Schenefeld, Germany, for provision of x-ray free-electron laser beamtime at the Scientific Instrument HED (High Energy Density Science) and would like to thank the staff for their assistance. We thank G. Geloni for the current information about the self-seeding performance of the European XFEL.

K.V., N.J.H., O.S.H., A.K.S., and D.K. were supported by the Helmholtz Association under No. VH-NG-1141 and O.S.H. was supported by the Helmholtz Association under Grant No. ERC-RA-0041. K.F. and M.S. were supported by the Helmholtz Association under Grant No. VH-NG-1338. K.R. acknowledges funding by the Center for Advanced Systems Understanding (CASUS) which is financed by the German Federal Ministry of Education and Research (BMBF) and by the Saxon Ministry for Science, Culture and Tourism (SMWK) with tax funds on the basis of the budget approved by the Saxon State Parliament. M.L. was supported by the German Federal Ministry of Education and Research (BMBF, No. 01/S18026A-F) by funding the competence center for Big Data and AI “ScaDS.AI Dresden/Leipzig.” N.J.H. and L.B.F. acknowledge support from the Department of Energy, Office of Science, Office of Fusion Energy Sciences under No. FWP 100182 and N.J.H. was supported by the Department of Energy, Laboratory Directed Research and Development program at SLAC National Accelerator Laboratory, under Contract No. DE-AC02-76SF00515. The work of T.D. and S.P.H.-R. was performed under the auspices of the U.S. Department of Energy by Lawrence Livermore National Laboratory under Contract No. DE-AC52-07NA27344 and T.D. was supported by Laboratory Directed Research and Development (LDRD) Grant No. 18-ERD-033. R.W.F. acknowledges support from the Department of Energy, National Nuclear Security Administration Award No. DE-NA0003842, and the Department of Energy, Office of Science, Office of Fusion Energy Sciences Award No. DE-SC0018298.

Computations were performed on a Bull Cluster at the Center for Information Services and High Performance Computing (ZIH) at Technische Universität Dresden, on the clusters hypnos and hemera at Helmholtz-Zentrum Dresden-Rossendorf (HZDR).

DATA AVAILABILITY

Raw data were generated at the European XFEL large scale facility. The data that support the findings of this study are available from the corresponding author upon reasonable request.

REFERENCES

- ¹Frontiers and Challenges in Warm Dense Matter, edited by F. Graziani, M. P. Desjarlais, R. Redmer, and S. B. Trickey (Springer International Publishing, 2014).
- ²D. Riley, *Plasma Phys. Controlled Fusion* **60**, 014033 (2017).
- ³M. S. Murillo, *Phys. Plasmas* **11**, 2964 (2004).
- ⁴M. Ross, *Nature* **292**, 435 (1981).
- ⁵D. Kraus, J. Vorberger, A. Pak, N. J. Hartley, L. B. Fletcher, S. Frydrych, E. Galtier, E. J. Gamboa, D. O. Gericke, S. H. Glenzer, E. Granados, M. J. MacDonald, A. J. MacKinnon, E. E. McBride, I. Nam, P. Neumayer, M. Roth, A. M. Saunders, A. K. Schuster, P. Sun, T. van Driel, T. Döppner, and R. W. Falcone, *Nat. Astron.* **1**, 606 (2017).
- ⁶A. L. Kritcher, D. C. Swift, T. Döppner, B. Bachmann, L. X. Benedict, G. W. Collins, J. L. DuBois, F. Elsner, G. Fontaine, J. A. Gaffney, S. Hamel, A. Lazicki, W. R. Johnson, N. Kostinski, D. Kraus, M. J. MacDonald, B. Maddox, M. E. Martin, P. Neumayer, A. Nikroo, J. Nilsen, B. A. Remington, D. Saumon, P. A. Sterne, W. Sweet, A. A. Correa, H. D. Whitley, R. W. Falcone, and S. H. Glenzer, *Nature* **584**, 51 (2020).
- ⁷J. H. Eggert, D. G. Hicks, P. M. Celliers, D. K. Bradley, R. S. McWilliams, R. Jeanloz, J. E. Miller, T. R. Boehly, and G. W. Collins, *Nat. Phys.* **6**, 40 (2009).
- ⁸M. Harmand, A. Ravasio, S. Mazevet, J. Bouchet, A. Denoëud, F. Dorchies, Y. Feng, C. Fourment, E. Galtier, J. Gaudin, F. Guyot, R. Kodama, M. Koenig, H. J. Lee, K. Miyanishi, G. Morard, R. Musella, B. Nagler, M. Nakatsutsumi, N.

- Ozaki, V. Recoules, S. Toleikis, T. Vinci, U. Zastra, D. Zhu, and A. Benuzzi-Mounaix, *Phys. Rev. B* **92**, 024108 (2015).
- ⁹F. Dorchies, F. Festa, V. Recoules, O. Peyrusse, A. Benuzzi-Mounaix, E. Brambrink, A. Levy, A. Rvasio, M. Koenig, T. Hall, and S. Mazevet, *Phys. Rev. B* **92**, 085117 (2015).
- ¹⁰R. Torchio, F. Ocelli, O. Mathon, A. Sollier, E. Lescoute, L. Videau, T. Vinci, A. Benuzzi-Mounaix, J. Headspith, W. Helsby, S. Bland, D. Eakins, D. Chapman, S. Pascarelli, and P. Loubeyre, *Sci. Rep.* **6**, 26402 (2016).
- ¹¹M. Guarguaglini, J.-A. Hernandez, T. Okuchi, P. Barroso, A. Benuzzi-Mounaix, M. Bethkenhagen, R. Bolis, E. Brambrink, M. French, Y. Fujimoto, R. Kodama, M. Koenig, F. Lefevre, K. Miyanishi, N. Ozaki, R. Redmer, T. Sano, Y. Umeda, T. Vinci, and A. Rvasio, *Sci. Rep.* **9**, 10155 (2019).
- ¹²N. J. Hartley, C. Zhang, X. Duan, L. G. Huang, S. Jiang, Y. Li, L. Yang, A. Pelka, Z. Wang, J. Yang, and D. Kraus, *Matter Radiat. Extremes* **5**, 028401 (2020).
- ¹³B. I. Cho, T. Ogitsu, K. Engelhorn, A. A. Correa, Y. Ping, J. W. Lee, L. J. Bae, D. Prendergast, R. W. Falcone, and P. A. Heimann, *Sci. Rep.* **6**, 18843 (2016).
- ¹⁴T. Kluge, M. Rödel, J. Metzkes-Ng, A. Pelka, A. L. Garcia, I. Prencipe, M. Rehwald, M. Nakatsutsumi, E. E. McBride, T. Schönherr, M. Garten, N. J. Hartley, M. Zacharias, J. Grenzer, A. Erbe, Y. M. Georgiev, E. Galtier, I. Nam, H. J. Lee, S. Glenzer, M. Bussmann, C. Gutt, K. Zeil, C. Rödel, U. Hübner, U. Schramm, and T. E. Cowan, *Phys. Rev. X* **8**, 031068 (2018).
- ¹⁵B. Mahieu, N. Jourdain, K. T. Phuoc, F. Dorchies, J.-P. Goddet, A. Lifschitz, P. Renaudin, and L. Lecherbourg, *Nat. Commun.* **9**, 3276 (2018).
- ¹⁶S. M. Vinko, O. Ciricosta, B. I. Cho, K. Engelhorn, H.-K. Chung, C. R. D. Brown, T. Burian, J. Chalupský, R. W. Falcone, C. Graves, V. Hájková, A. Higginbotham, L. Juha, J. Krzywinski, H. J. Lee, M. Messerschmidt, C. D. Murphy, Y. Ping, A. Scherz, W. Schlöter, S. Toleikis, J. J. Turner, L. Vysin, T. Wang, B. Wu, U. Zastra, D. Zhu, R. W. Lee, P. A. Heimann, B. Nagler, and J. S. Wark, *Nature* **482**, 59 (2012).
- ¹⁷S. P. Hau-Riege, A. Graf, T. Döppner, R. A. London, J. Krzywinski, C. Fortmann, S. H. Glenzer, M. Frank, K. Sokolowski-Tinten, M. Messerschmidt, C. Bostedt, S. Schorb, J. A. Bradley, A. Lutman, D. Rolles, A. Rudenko, and B. Rudek, *Phys. Rev. Lett.* **108**, 217402 (2012).
- ¹⁸D. Kraus, B. Bachmann, B. Barbrel, R. W. Falcone, L. B. Fletcher, S. Frydrych, E. J. Gamboa, M. Gauthier, D. O. Gericke, S. H. Glenzer, S. Göde, E. Granados, N. J. Hartley, J. Helfrich, H. J. Lee, B. Nagler, A. Rvasio, W. Schumaker, J. Vorberger, and T. Döppner, *Plasma Phys. Controlled Fusion* **61**, 014015 (2018).
- ¹⁹B. Y. Sharkov, D. H. H. Hoffmann, A. A. Golubev, and Y. Zhao, *Matter Radiat. Extremes* **1**, 28 (2016).
- ²⁰N. J. Hartley, S. Brown, T. E. Cowan, E. Cunningham, T. Döppner, R. W. Falcone, L. B. Fletcher, S. Frydrych, E. Galtier, E. J. Gamboa, A. L. Garcia, D. O. Gericke, S. H. Glenzer, E. Granados, P. A. Heimann, H. J. Lee, M. J. MacDonald, A. J. MacKinnon, E. E. McBride, I. Nam, P. Neumayer, A. Pak, A. Pelka, I. Prencipe, A. Rvasio, M. Rödel, K. Rohatsch, A. M. Saunders, M. Schölmerich, M. Schörner, A. K. Schuster, P. Sun, T. van Driel, J. Vorberger, and D. Kraus, *Sci. Rep.* **9**, 4196 (2019).
- ²¹D. Kraus, N. J. Hartley, S. Frydrych, A. K. Schuster, K. Rohatsch, M. Rödel, T. E. Cowan, S. Brown, E. Cunningham, T. van Driel, L. B. Fletcher, E. Galtier, E. J. Gamboa, A. L. Garcia, D. O. Gericke, E. Granados, P. A. Heimann, H. J. Lee, M. J. MacDonald, A. J. MacKinnon, E. E. McBride, I. Nam, P. Neumayer, A. Pak, A. Pelka, I. Prencipe, A. Rvasio, R. Redmer, A. M. Saunders, M. Schölmerich, M. Schörner, P. Sun, S. J. Turner, A. Zettl, R. W. Falcone, S. H. Glenzer, T. Döppner, and J. Vorberger, *Phys. Plasmas* **25**, 056313 (2018).
- ²²S. H. Glenzer, G. Gregori, R. W. Lee, F. J. Rogers, S. W. Pollaine, and O. L. Landen, *Phys. Rev. Lett.* **90**, 175002 (2003).
- ²³S. H. Glenzer, O. L. Landen, P. Neumayer, R. W. Lee, K. Widmann, S. W. Pollaine, R. J. Wallace, G. Gregori, A. Höll, T. Bornath, R. Thiele, V. Schwarz, W.-D. Kraeft, and R. Redmer, *Phys. Rev. Lett.* **98**, 065002 (2007).
- ²⁴A. L. Kritcher, P. Neumayer, J. Castor, T. Döppner, R. W. Falcone, O. L. Landen, H. J. Lee, R. W. Lee, E. C. Morse, A. Ng, S. Pollaine, D. Price, and S. H. Glenzer, *Science* **322**, 69 (2008).
- ²⁵L. B. Fletcher, H. J. Lee, T. Döppner, E. Galtier, B. Nagler, P. Heimann, C. Fortmann, S. LePape, T. Ma, M. Millot, A. Pak, D. Turnbull, D. A. Chapman, D. O. Gericke, J. Vorberger, T. White, G. Gregori, M. Wei, B. Barbrel, R. W. Falcone, C.-C. Kao, H. Nuhn, J. Welch, U. Zastra, P. Neumayer, J. B. Hastings, and S. H. Glenzer, *Nat. Photonics* **9**, 274 (2015).
- ²⁶P. Davis, T. Döppner, J. R. Rygg, C. Fortmann, L. Divol, A. Pak, L. Fletcher, A. Becker, B. Holst, P. Sperling, R. Redmer, M. P. Desjarlais, P. Celliers, G. W. Collins, O. L. Landen, R. W. Falcone, and S. H. Glenzer, *Nat. Commun.* **7**, 11189 (2016).
- ²⁷S. Frydrych, J. Vorberger, N. J. Hartley, A. K. Schuster, K. Ramakrishna, A. M. Saunders, T. van Driel, R. W. Falcone, L. B. Fletcher, E. Galtier, E. J. Gamboa, S. H. Glenzer, E. Granados, M. J. MacDonald, A. J. MacKinnon, E. E. McBride, I. Nam, P. Neumayer, A. Pak, K. Voigt, M. Roth, P. Sun, D. O. Gericke, T. Döppner, and D. Kraus, *Nat. Commun.* **11**, 2620 (2020).
- ²⁸K. Falk, E. J. Gamboa, G. Kagan, D. S. Montgomery, B. Srinivasan, P. Tzeferacos, and J. F. Benage, *Phys. Rev. Lett.* **112**, 155003 (2014).
- ²⁹S. L. Pape, P. Neumayer, C. Fortmann, T. Döppner, P. Davis, A. Kritcher, O. Landen, and S. Glenzer, *Phys. Plasmas* **17**, 056309 (2010).
- ³⁰E. J. Gamboa, L. B. Fletcher, H. J. Lee, U. Zastra, E. Galtier, M. J. MacDonald, M. Gauthier, J. Vorberger, D. O. Gericke, E. Granados, J. B. Hastings, and S. H. Glenzer, *Phys. Plasmas* **22**, 056319 (2015).
- ³¹D. Kraus, A. Rvasio, M. Gauthier, D. O. Gericke, J. Vorberger, S. Frydrych, J. Helfrich, L. B. Fletcher, G. Schaumann, B. Nagler, B. Barbrel, B. Bachmann, E. J. Gamboa, S. Göde, E. Granados, G. Gregori, H. J. Lee, P. Neumayer, W. Schumaker, T. Döppner, R. W. Falcone, S. H. Glenzer, and M. Roth, *Nat. Commun.* **7**, 10970 (2016).
- ³²E. Principi, S. Krylow, M. E. Garcia, A. Simoncig, L. Foglia, R. Mincigrucci, G. Kurdi, A. Gessini, F. Bencivenga, A. Giglia, S. Nannarone, and C. Masciovecchio, *Phys. Rev. Lett.* **125**, 155703 (2020).
- ³³U. Bergmann, P. Glatzel, and S. P. Cramer, *Microchem. J.* **71**, 221 (2002).
- ³⁴C. J. Sahle, A. Mirone, J. Niskanen, J. Inkinen, M. Krisch, and S. Huotari, *J. Synchrotron Radiat.* **22**, 400 (2015).
- ³⁵W. Schülke, *Electron Dynamics by Inelastic X-Ray Scattering* (Oxford University Press, 2007), Vol. 7.
- ³⁶D. Sokaras, D. Nordlund, T.-C. Weng, R. A. Mori, P. Velikov, D. Wenger, A. Garachtchenko, M. George, V. Borzenets, B. Johnson, Q. Qian, T. Rabedeau, and U. Bergmann, *Rev. Sci. Instrum.* **83**, 043112 (2012).
- ³⁷S. Huotari, C. J. Sahle, C. Henriquet, A. Al-Zein, K. Martel, L. Simonelli, R. Verbeni, H. Gonzalez, M.-C. Lagier, C. Ponchut, M. M. Sala, M. Krisch, and G. Monaco, *J. Synchrotron Radiat.* **24**, 521 (2017).
- ³⁸D. J. Bowron, M. H. Krisch, A. C. Barnes, J. L. Finney, A. Kaprolat, and M. Lorenzen, *Phys. Rev. B* **62**, R9223 (2000).
- ³⁹W. L. Mao, H. Kwang Mao, P. J. Eng, T. P. Trainor, M. Newville, C. Chang Kao, D. L. Heinz, J. Shu, Y. Meng, and R. J. Hemley, *Science* **302**, 425 (2003).
- ⁴⁰S. K. Lee, Y.-H. Kim, Y. S. Yi, P. Chow, Y. Xiao, C. Ji, and G. Shen, *Phys. Rev. Lett.* **123**, 235701 (2019).
- ⁴¹C. Weis, G. Spiekermann, C. Sternemann, M. Harder, G. Vankó, V. Cerantola, C. J. Sahle, Y. Forov, R. Sakrowski, I. Kupenko, S. Petitgirard, H. Yavaş, C. Bressler, W. Gawelda, M. Tolan, and M. Wilke, *J. Anal. At. Spectrom.* **34**, 384 (2019).
- ⁴²S. Galambosi, J. A. Soininen, K. Nygård, S. Huotari, and K. Hämäläinen, *Phys. Rev. B* **76**, 195112 (2007).
- ⁴³S. Huotari, T. Pylkkänen, J. A. Soininen, J. J. Kas, K. Hämäläinen, and G. Monaco, *J. Synchrotron Radiat.* **19**, 106 (2012).
- ⁴⁴M. Nakatsutsumi, K. Appel, G. Priebe, I. Thorpe, A. Pelka, B. Müller, and T. Tschentscher, "Technical design report: Scientific instrument high energy density physics (HED)," Technical Report No. XFEL EU TR-2014-001 (European X-Ray Free-Electron Laser Facility GmbH, 2014).
- ⁴⁵U. Zastra, M. McMahon, K. Appel, C. Baehtz, E. Brambrink, R. Briggs, T. Butcher, B. Cauble, B. Chen, H. Damker, C. Deiter, L. Eggert, K. Falk, L. B. Fletcher, S. H. Glenzer, S. Göde, M. Harmand, A. Higginbotham, Z. Konöpková, D. Kraus, H.-P. Liermann, M. Nakatsutsumi, A. Pelka, G. Priebe, R. Redmer, A. Schropp, R. Smith, P. Sperling, I. Thorpe, and S. Toleikis, "Conceptual design report: Dynamic laser compression experiments at the HED instrument of European XFEL," Technical Report No. XFEL EU TR-2017-001 (European X-Ray Free-Electron Laser Facility GmbH, 2017).
- ⁴⁶J. H. Beaumont and M. Hart, *J. Phys. E* **7**, 823 (1974).
- ⁴⁷T. R. Preston, S. Göde, J.-P. Schwinkendorf, K. Appel, E. Brambrink, V. Cerantola, H. Höppner, M. Makita, A. Pelka, C. Prescher, K. Sukharnikov, A. Schmidt, I. Thorpe, T. Toncian, A. Amouretti, D. Chekrygina, R. W. Falcone, K. Falk, L. B. Fletcher, E. Galtier, M. Harmand, N. J. Hartley, S. P. Hau-Riege, P. Heimann, L. G. Huang, O. S. Humphries, O. Karnbach, D. Kraus, H. J. Lee,

- B. Nagler, S. Ren, A. K. Schuster, M. Smid, K. Voigt, M. Zhang, and U. Zastra, *J. Instrum.* **15**, P11033 (2020).
- ⁴⁸A. Mozzanica, A. Bergamaschi, M. Brueckner, S. Cartier, R. Dinapoli, D. Greiffenberg, J. Jungmann-Smith, D. Maliakal, D. Mezza, M. Ramilli, C. Ruder, L. Schaedler, B. Schmitt, X. Shi, and G. Tinti, *J. Instrum.* **11**, C02047 (2016).
- ⁴⁹K. Nishimura, G. Blaj, P. Caragiulo, G. Carini, A. Dragone, G. Haller, P. Hart, J. Hasi, R. Herbst, S. Herrmann, C. Kenney, M. Kwiatkowski, B. Markovic, S. Osier, J. Pines, B. Reese, J. Segal, A. Tomada, and M. Weaver, *AIP Conf. Proc.* **1741**, 040047 (2016).
- ⁵⁰See Andor, <https://andor.oxinst.com/products/scmos-camera-series/zyla-5-5-scmos> for “Zyla 5.5 sCMOS” (last accessed 18 February, 2021).
- ⁵¹A. Descamps, B. K. Ofori-Okai, K. Appel, V. Cerantola, A. Comley, J. H. Eggert, L. B. Fletcher, D. O. Gericke, S. Göde, O. Humphries, O. Karnbach, A. Lazicki, R. Loetzsch, D. McGonagle, C. A. J. Palmer, C. Plueckthun, T. R. Preston, R. Redmer, D. G. Senesky, C. Strohm, I. Uschmann, T. G. White, L. Wollenweber, G. Monaco, J. S. Wark, J. B. Hastings, U. Zastra, G. Gregori, S. H. Glenzer, and E. E. McBride, *Sci. Rep.* **10**, 14564 (2020).
- ⁵²A. Pak, G. Gregori, J. Knight, K. Campbell, D. Price, B. Hammel, O. L. Landen, and S. H. Glenzer, *Rev. Sci. Instrum.* **75**, 3747 (2004).
- ⁵³Y. Joly, *Phys. Rev. B* **63**, 125120 (2001).
- ⁵⁴O. Bunău and Y. Joly, *J. Phys.* **21**, 345501 (2009).
- ⁵⁵G. S. Painter, D. E. Ellis, and A. R. Lubinsky, *Phys. Rev. B* **4**, 3610 (1971).
- ⁵⁶W. Schülke, U. Bonse, H. Nagasawa, A. Kaprolat, and A. Berthold, *Phys. Rev. B* **38**, 2112 (1988).
- ⁵⁷G. Kresse and J. Hafner, *Phys. Rev. B* **47**, 558 (1993).
- ⁵⁸G. Kresse and J. Furthmüller, *Phys. Rev. B* **54**, 11169 (1996).
- ⁵⁹G. Kresse and J. Furthmüller, *Comput. Mater. Sci.* **6**, 15 (1996).
- ⁶⁰G. Kresse and D. Joubert, *Phys. Rev. B* **59**, 1758 (1999).
- ⁶¹S. Nosé, *J. Chem. Phys.* **81**, 511 (1984).
- ⁶²W. G. Hoover, *Phys. Rev. A* **31**, 1695 (1985).
- ⁶³J. P. Perdew, K. Burke, and M. Ernzerhof, *Phys. Rev. Lett.* **77**, 3865 (1996).
- ⁶⁴H. J. Monkhorst and J. D. Pack, *Phys. Rev. B* **13**, 5188 (1976).
- ⁶⁵P. Vinet, J. R. Smith, J. Ferrante, and J. H. Rose, *Phys. Rev. B* **35**, 1945 (1987).
- ⁶⁶P. Vinet, J. H. Rose, J. Ferrante, and J. R. Smith, *J. Phys.* **1**, 1941 (1989).
- ⁶⁷K. Ramakrishna and J. Vorberger, *J. Phys.* **32**, 095401 (2019).
- ⁶⁸E. J. Gamboa, L. B. Fletcher, H. J. Lee, M. J. MacDonald, U. Zastra, M. Gauthier, D. O. Gericke, J. Vorberger, E. Granados, J. B. Hastings, and S. H. Glenzer, “Band gap opening in strongly compressed diamond observed by x-ray energy loss spectroscopy,” Technical Report No. SLAC-PUB-16488 (SLAC National Accelerator Laboratory, 2016).
- ⁶⁹L. X. Benedict, K. P. Driver, S. Hamel, B. Militzer, T. Qi, A. A. Correa, A. Saul, and E. Schwegler, *Phys. Rev. B* **89**, 224109 (2014).
- ⁷⁰N. J. Hartley, J. Grenzer, L. Huang, Y. Inubushi, N. Kamimura, K. Katagiri, R. Kodama, A. Kon, W. Lu, M. Makita, T. Matsuoka, S. Nakajima, N. Ozaki, T. Pikuz, A. V. Rode, D. Sagae, A. K. Schuster, K. Tono, K. Voigt, J. Vorberger, T. Yabuuchi, E. E. McBride, and D. Kraus, *Phys. Rev. Lett.* **126**, 015703 (2021).
- ⁷¹I. Prencipe, J. Fuchs, S. Pascarelli, D. W. Schumacher, R. B. Stephens, N. B. Alexander, R. Briggs, M. Büscher, M. O. Cernaianu, A. Choukourov, M. D. Marco, A. Erbe, J. Fassbender, G. Fiquet, P. Fitzsimmons, C. Gheorghiu, J. Hund, L. G. Huang, M. Harmand, N. J. Hartley, A. Irman, T. Kluge, Z. Konopkova, S. Kraft, D. Kraus, V. Leca, D. Margarone, J. Metzkes, K. Nagai, W. Nazarov, P. Lutoslawski, D. Papp, M. Passoni, A. Pelka, J. P. Perin, J. Schulz, M. Smid, C. Spindloe, S. Steinke, R. Torchio, C. Vass, T. Wiste, R. Zaffino, K. Zeil, T. Tschtsentscher, U. Schramm, and T. E. Cowan, *High Power Laser Sci. Eng.* **5**, e17 (2017).
- ⁷²J. Amann, W. Berg, V. Blank, F.-J. Decker, Y. Ding, P. Emma, Y. Feng, J. Frisch, D. Fritz, J. Hastings, Z. Huang, J. Krzywinski, R. Lindberg, H. Loos, A. Lutman, H.-D. Nuhn, D. Ratner, J. Rzepliela, D. Shu, Y. Shvydko, S. Spampinati, S. Stoupin, S. Terentyev, E. Trakhtenberg, D. Walz, J. Welch, J. Wu, A. Zholents, and D. Zhu, *Nat. Photonics* **6**, 693 (2012).
- ⁷³G. Geloni, J. Anton, V. Blank, W. Decking, X. Dong, S. Karabekyan, S. Kearney, V. Kocharyan, D. La Civita, S. Liu, E. Negodin, E. Saldin, L. Samoylova, S. Serkez, R. Shayduk, D. Shu, H. Sinn, V. Sleziona, S. Terentiev, M. Vannoni, T. Wohlenberg, and M. Yakopov, in Proceedings of the 39th Free Electron Laser Conference FEL2019, Germany (2019).
- ⁷⁴G. Geloni, personal communication (25 May 2021).
- ⁷⁵S. Banerjee, K. Ertel, P. D. Mason, P. J. Phillips, M. D. Vido, J. M. Smith, T. J. Butcher, C. Hernandez-Gomez, R. J. S. Greenhalgh, and J. L. Collier, *Opt. Express* **23**, 19542 (2015).